Published in Catalysis Today, vol. 114, pp. 174-182 (2006)
http://dx.doi.org/10.1016/j.cattod.2006.01.014

Effect of fluorine-containing chiral templates on Mg distribution in the structure of MgAPO-5 and its influence on catalytic activity.

L. Gómez-Hortigüela[a,b], C. Márquez-Álvarez[a], E. Sastre[a], F. Corà[b] and J. Pérez-Pariente[a,*].

[a]Instituto de Catálisis y Petroleoquímica. C/ Marie Curie 2. 28049 Cantoblanco. Madrid. Spain. * Corresponding author: jperez@icp.csic.es

[b]Davy Faraday Research Laboratory. The Royal Institution of Great Britain. 21 Albemarle Street, London W1S 4BS, United Kingdom.

Abstract

MgAPO-5 materials have been synthesized by using three new structure directing agents: S-(-)-1-benzyl-2-pyrrolidinemethanol, and its ortho and meta-fluoro-benzyl derivatives. Their acidity has been measured and their catalytic activity tested in the cyclohexene oxide opening acid-catalyzed reaction. The catalytic activity of these materials can be related to their acidity. It has been found that MgAPO-5 samples synthesized from both fluorinated structure directing agents are much more active as acid catalysts for the reaction. A computational study based on molecular mechanics shows a rigid arrangement of the organic molecules in form of helices of dimers within the AFI structure, and suggests a direction of the fluorinated molecules towards the incorporation of magnesium atoms in the framework.

Keywords: magnesium distribution, enantioselectivity, structure directing effect, helicoidal arrangement, MgAPO-5.

Introduction

In contrast with the widespread utilization of molecular sieve catalysts in a large variety of commercial chemical processes, there is a paradoxical lack of effective control over siting and spatial distribution at Ångström scale of the active sites in the framework. The development of effective strategies for controlling the active sites distribution would no doubt have a strong impact on catalyst activity and selectivity, as it is well known that, at least for zeolite acid catalysts, the stability and intrinsic activity of the acid sites is governed by their local geometry and chemical environment [1,2,3].

Due to the ever increasing diversification and complexity of zeolite materials topologies, there is little chance of finding simple and general procedures to master the distribution of active sites applicable to every sort of crystalline molecular sieve. However, any advance and new insights in this field would make more feasible the final objective of tailoring the web of active sites present in the framework for specific catalytic requirements.

As most of the zeolite materials of interest in catalysis are synthetic in nature, the most straightforward way of gaining control over the active sites distribution would involve the appropriate manipulation of the synthesis parameters. In the particular case of aluminophosphates, of interest to this work, the presence of organic molecules in the synthesis gel is with almost no exception required to crystallize virtually every known structure of low framework density. We have reported elsewhere [4] that benzyl derivatives of several cyclic amines like pyrrolidine behave as convenient structure directing agents for the crystallization of the large-pore material AlPO-5 (AFI topology). Computational work has shown that the benzylpyrrolidine molecules arrange inside the AFI channels by forming dimers through the interaction of the respective aromatic rings [5]. Moreover, the replacement of just one hydrogen atom of the aromatic ring by one fluorine atom increases the interaction energy of the template with the framework. The dimers are able to rotate along the channel

axis, but is has been shown recently that the rotation is impeded by introducing a methanol group in alpha position of the pyrrolidine ring [6]. This is an interesting result, as it has been argued that avoiding "free" rotation of the SDA within one-dimensional channels of zeolites like ZSM-12 would enable to control the distribution of aluminium in the framework [7].

In this work we have explored the possibility of controlling the magnesium distribution in MgAPO-5 crystals by using fluorine-containig S-(-)-1-benzyl-2-pyrrolidinemethanol (bpm) derivatives as structure directing agents (SDAs). The influence of the chemical nature of the SDA molecule over acidity and catalytic activity of the calcined materials in acid-catalyzed reactions will be studied.

A further issue that will be investigated here concerns the potential catalytic consequences of using an enantiomerically pure chiral template, as bpm, in the synthesis. Calculations based on molecular mechanics show the chiral bpm template molecules to adopt an helicoidal configuration along the AFI channel [6]. If the Mg distribution in the 6-MR that build up the 12-MR channel walls is indeed governed by the spatial configuration of the dimeric template units, then an helicoidal arrangement of Mg cations along the channel would eventually be also present in the crystals. The reaction of cyclohexene oxide with ethanol (scheme 1) to obtain the corresponding derivatives (**2**) that contain two asymmetric carbon atoms has been used as chiral test reaction.

Experimental

Synthesis and characterization of MgAPO-5 materials

S-(-)-1-benzyl-2-pyrrolidinemethanol and its fluorinated derivatives were synthesized starting from L-proline (Aldrich, 99+%) in two steps: reduction of the acid moiety with $LiAlH_4$ (Aldrich, 95%) to give L-prolinol, and subsequent alkylation of the amino group with the corresponding benzyl (Aldrich, 97%) or ortho- or meta-fluoro benzyl (Avocado, 98%)

chloride to yield the desired product. These molecules were purified by vacuum distillation and characterized by CCF and EA.

MgAPO materials were prepared starting from gels with the following molar composition: 1R : P_2O_5 : 0,89 Al_2O_3 : 0,22 MgO : 40 H_2O, where R stands for the organic molecule, triethylamine (TEA), S-(-)-1-benzyl-2-pyrrolidinemethanol (bpm), S-(-)-1-orthofluorobenzyl-2-pyrrolidinemethanol (ofbpm) and S-(-)-1-metafluorobenzyl-2-pyrrolidinemethanol (mfbpm). The gels were prepared by adding the aluminium source, pseudoboehmite (Catapal Pural SB, 75.3% wt Al_2O_3) and the magnesium source, $Mg(CH_3COO)_2{\cdot}4H_2O$ (Sigma-Aldrich, 99%), to a solution of phosphoric acid (Riedel-de Haen, 85% wt) and water and stirred for 1 hour in a closed recipient (having a hole for the stirrer). The amine was then added, and the stirring maintained for 2 hours. The pH of the resulting gels was between 3.5 and 4.0.

The respective gels were introduced into 60 ml teflon lined stainless steel autoclaves and heated statically at 423 K for 3 days. The resulting solids were separated by filtration, washed with ethanol and water and dried at 333 K overnight.

Calcination of the MgAPO-5 samples were carried out by passing an oxygen stream enriched in ozone (3-4%) at 473 K for 96 hours. Complete removal of the organic was verified by TGA and IR spectroscopy.

The solid products were characterized by XRD (Seifert XRD 3000P diffractometer, CuKα radiation), thermal analysis (Perkin-Elmer TGA7 instrument, heating rate 10º/min, air flow 30 ml/min), chemical analysis (Perkin-Elmer 2400 CHN analyzer; ICP Plasma for aluminum, phosphorus, magnesium), SEM/EDX (JEOL JM-6400 operating at 20 kV) and solid state Nuclear Magnetic Resonance. MAS NMR spectra were recorded with a Bruker AV 400 WB spectrometer, using a BL7 probe for ^{13}C, a BL4 probe for ^{31}P and ^{27}Al, and a BL2.5 probe for ^{19}F. ^{1}H to ^{13}C cross polarization (CP) spectra were recorded using π/2 rad pulses of 4.5 μs for

^{1}H, a contact time of 5 ms and a recycle delay of 3 s. For the acquisition of the ^{13}C spectra, the samples were span at the magic angle (MAS) at a rate of 5-5.5 kHz. For ^{31}P, $\pi/2$ rad pulses of 4.25 μs and recycle delays of 80 s were used. The ^{27}Al spectra were measured using pulses of 1 μs to flip the magnetization $\pi/12$ rad, and delays of 1s between two consecutives pulses. Both ^{31}P and ^{27}Al spectra were recorded while spinning the samples at c. a. 11 kHz. For ^{19}F, $\pi/2$ pulses of 4.5 μs recycle delays of 80 s and spinning rates of approximately 20 kHz were used.

Acidity measurements

For infrared measurements, the samples were pressed into thin self-supporting wafers (thickness, ca. 8 $mg \cdot cm^{-2}$) and activated in vacuum (10^{-3} Pa) at 623 K for 9 h in a glass IR cell with CaF_2 windows. Pyridine (analytical grade, Fluka) was subsequently dosed (8 Torr) and the samples kept at 423 K for 90 min to allow diffusion to all accessible sites. After pyridine adsorption, succesive evacuation treatments at 423, 523 and 623 K for 1 h under dynamic vacuum were performed. Infrared spectra were recorded after activation and after each evacuation treatment using a Nicolet 5ZDX FTIR spectrometer provided with an MCT detector. Spectra in the 4000-1000 cm^{-1} range were acquired at 4 cm^{-1} resolution by averaging 250 scans and using Happ-Genzel apodization.

Catalytic tests

MgAPO solids were tested as catalysts for the epoxide ring opening of cyclohexene oxide (98 %, Aldrich) (**1**) with ethanol (99.5 %, Aldrich) -Scheme 1-. Reactions were carried out at 353 K in a 25 ml magnetically stirred, round-bottomed flask. 1-Tetradecane (99 %, Sigma) was chosen as internal standard. The reagents mixture was 5.5/1.0 molar ratio of cyclohexene oxide to ethanol with 5-6 wt. % catalyst load. Aliquots were taken at regular time intervals.

The ring opening product of the reaction, trans-2-ethoxi-cyclohexanol (**2**), which possesses two chiral carbon atoms, is the main compound observed, and only when the cyclohexene

oxide conversion is high or the reaction time is prolonged, traces of trans-1,2-diethoxi-cyclohexane are observed.

The composition of the reacting mixture was periodically analyzed by GC using a Fisons 8000 Series device, equipped with a Tracer^{TM} capillary column covered with Tracsil-TR-WAX, with 60 m x 0.25 mm x 0.25 μm dimensions, connected to a FID detector. Helium was used as carrier gas.

The analyses of the enantiomer selectivities were performed in a Hewlett-Packard 5890 II Gas Chromatograph equipped with a chiral glass capillary column (mixture of methyl silicone -OV-1701- and methylsilicone-heptakis-[2,3-dipentyl-6-(tert-butyldimethylsilyl)]-b-cyclodextrin as stationary phase), according to [8].

Results

The bpm molecule, either non fluorinated or containing fluorine atoms in meta or ortho position of the aromatic ring, allows the synthesis of highly crystalline AlPO-5 and MgAPO-5 samples, as illustrated in figure 1. The Mg/(Mg+P+Al) molar fraction of the solid, determined by ICP is 0.05, which is only slightly lower than that of the synthesis gel (0.055). From this value a Mg content of 1.2 atoms per unit cell (u.c.) for all the samples is obtained (Table 1), regardless of the presence or position of the fluorine atom in the template molecule. This value is slighlty lower than that of MgAPO-5 crystals obtained from gels containing triethylamine (TEA). TG analyses of representative samples (figure 2) show the release of the organic molecule occluded inside the AFI channels to occur in three different steps between 453 and 923 K for AlPO-5, while removal of all organic material from MgAPO-5 requires heating the sample up to ~ 1093 K. This temperature increase is also observed for MgAPO-5 synthesized from triethylamine [9], and it is generally taken as an evidence of the presence of Mg in the framework. The weight loss below 453 K corresponds to the desorption of water. The organic content determined by TG is around 13 wt % in all cases, which corresponds to

1.1 molecules per unit cell (table 1). Furthermore, this value matches the Mg content of the crystals, evidencing that the organic molecules are protonated, as required for charge balance.

The presence of Mg in the framework of the as-made materials has also been evidenced by ^{31}P MAS-NMR (figure 3, left). The spectra of the MgAPO-5 samples show two resonance signals at –30 ppm and –24 ppm, assigned to P(4Al) and P(3Al,1Mg) environments, respectively. Deconvolution of the spectra allows us to determine the molar fraction of Mg cations present in the framework, and a value between 1.1 and 1.2 Mg/u.c. is obtained for all the samples, which is in very good agreement with that determined by chemical analysis. This result evidences that all Mg is incorporated in the framework. ^{27}Al MAS-NMR spectra (figure 3, right) show an intense peak around 37 ppm, characteristic of tetrahedral aluminum in aluminophosphates; an additional signal of much lower intensity is also detected around 7 ppm. This signal could be due to minor amounts of unreacted pseudoboehmite present in the solid, or to pentacoordinated aluminum due to the coordination of framework aluminum with one water molecule [10].

The presence of the bpm molecules in the material has been assessed by ^{13}C NMR spectroscopy. ^{13}C CP-MAS-NMR spectra of the MgAPO-5 samples synthesized with the non-fluorinated, mfbpm and ofbpm molecules are shown in figure 4. The signal at 24 ppm corresponds to the CH_2 groups in beta position of the pyrrolidine ring, while those in alpha position as well as the benzyl CH_2 group contribute to the signal around 60 ppm; the signal at 68 ppm corresponds to the CH_2OH moiety. The peak at 133 ppm corresponds to the carbon atoms of the aromatic ring; this signal splits into three resonance lines by replacing one hydrogen atom by one fluorine atom in the aromatic ring either in meta or ortho position. Moreover, the fluorinated molecules give an additional peak at 160 ppm assigned to the aromatic carbon bonded to the fluorine atom. The ^{19}F MAS-NMR spectra of the MgAPO-5 samples show the presence of signals at –108 ppm and –118 ppm for the samples prepared

from the meta and ortho-fluoro derivatives, respectively, and are assigned to fluorine atoms bonded to carbon atoms of the aromatic ring [11,12,13]. Therefore, these spectra confirm the presence of unaltered bpm molecules inside the AFI channels of these materials.

Computational study

We have previously shown that benzylpyrrolidine molecules and derivatives self-assemble into densely packed dimers, which are the true structure directing agents during the synthesis of the AFI-type materials [5]. Moreover, we rationally designed a modified SDA, S-(-)-1-benzyl-2-pyrrolidinemethanol (bpm), in order to achieve a chiral supramolecular arrangement of the SDAs inside the microporous structure. Molecular dynamics studies of the protonated bpm molecules based on molecular mechanics (cvff [14] forcefield) have demonstrated the chiral self-assembly of these SDA cations inside the structure to form an helicoidal arrangement of the dimers [6]; the most stable configuration occurs when adjacent dimers are rotated by the same angle of –90º relative to each other, which yield an optimal fitting between the substituted pyrrolidine rings.

The same computational methodology has been applied to the fluorinated SDAs studied in the present work, ofbpm and mfbpm. The same chiral self-assemblies in form of dimers rotated by –90º have been found for both fluorinated SDA cations, as expected since the -CH_2OH substituent of the pyrrolidine ring, which is the reason for the preferred rotation, is the same in each molecule. Therefore, these molecules are also predicted to form an helicoidal, and hence chiral, arrangements within the AFI-type structure. The question that arises for the present study is wether this helicoidal arrangement of the fluorinated SDAs will affect the incorporation of the Mg dopants.

First, we studied the mobility of the helicoidal arrangement of SDA molecules inside the channels. To this goal, we ran 100 ps of MD calculations at 423 K (synthesis temperature) for a fully loaded and long-range ordered periodic system composed of 24 molecules in 18 u.c.,

corresponding to three complete pitches of the helix, in order to remove constraints imposed by the periodic boundary conditions. Analysis of the internal coordinates as a function of the simulation time is employed to monitor the mobility of the SDA molecules. We found that translation along the c axis is completely restricted, since it requires the simultaneous translation of the complete SDA helix. Rotation around the c axis is in principle less restricted. Two different types of rotational movement are allowed: rotation of a single dimeric SDA unit, and rotation of the complete helix around the c axis. To study the first movement, we monitored the relative rotation angles between subsequent dimers as a function of the MD time. Inter-dimer angles are also a measure of the rigidity of the helix, and yield information about the possibility of dimers to rotate independently around the c axis, breaking the helix. Rotation of the complete helix was instead studied by measuring the angle between the aromatic ring of one of the molecules and one of the 6MR rings of the channel walls.

Results are presented in figure 5 (results shown only for bpm). None of the angles between consecutive dimers varies during the simulation: all of them remain as –90º (figure 5, color lines). For all three derivatives (bpm, ofbpm and mfbpm) we found that the rotation of one dimer is restricted. It involves the breaking of the helix, and requires an high activation energy. This result indicates the stability of the helix, and the high energetic cost associated with its breaking. Therefore, we conclude that the helicoidal arrangements are very rigid: once the helices are formed, they stay in the same configuration with all the dimers rotated by the same angle of –90º.

Also the rotation of the complete helix is restricted, since the angle between one of the dimers and one of the 6MR of the channel walls does not vary at all (figure 5, black line). Our first conclusion is therefore that helices formed by fluorinated as well as non-fluorinated bpm derivatives are rigid, and their movement, both translational along the channel direction and rotational around the channel axis, is totally restricted. This restriction of mobility could

favour an ordered inclusion of the dopants within the AFI walls, provided a strong association is established between dopant and SDA molecules during the synthesis.

To investigate if this is the case, we calculated the relative energy of different local configurations of dopant and SDA cations, consisting of location of one Mg dopant in the framework and orientation of the SDA dimer relative to the dopant. A simple, but computationally efficient model has been chosen for this initial test. It consists of 5 u.c. of AFI where one dimer was loaded, and two argon atoms were inserted at its extremes in order to preserve the inter-molecular distance during the simulations (figure 6, left). One Mg ion substitued one aluminium in the region of the framework in front of the SDA dimer; two possible non-equivalent Mg positions were studied, named Mg-2 and Mg-1 (figure 6, left). In the Mg-2 position, the interaction of Mg with the SDA occurs mainly with the substituted pyrrolidine ring; in Mg-1 with the benzyl rings. We studied the rotation of the dimers around the c axis (figure 7), to identify possible preferred orientations of the SDA dimers relative to Mg. All possible orientations were studied for each rotation, and the most stable situations were plotted. Results for the Mg-1 position are plotted in figure 7 and show that for bpm several configurations have comparable stability; only one orientation is unstable, which corresponds to the CH_2OH substituent facing the Mg ion. Thus, there is not a remarked preferred orientation of bpm with respect to the dopant in Mg-1 positions. However, for ofbpm and mfbpm, different relative orientations have large differences in interaction energy; in addition, one orientation is much more stable than the others. This corresponds to the negatively charged fluorine atoms being located on the opposite side of the channel with respect to the low valent Mg dopant. This orientation minimizes the electrostatic repulsion (figure 7, right). For the Mg-2 position, only the ofbpm showed a clear preferred orientation, corresponding to both fluorine and methanol substituents being opposite to the Mg position; nevertheless, the energy differences were smaller than those for the Mg-1 position. This lower

influence of the dimer orientation, especially in the mfbpm molecule, towards the location of Mg in the Mg-2 position is due to the longer distance between fluorine atoms and Mg-2.

Therefore, the presence of fluorine substituents in the SDA, especially in the ortho position, causes a strong association between molecules and dopants; the negative atomic charge of fluorine atoms causes a strong electrostatic repulsion with the net negative charge associated to the incorporation of Mg, especially when it is located in Mg-1 position, which could direct the incorporation of such dopant atoms. This feature, together with the rigidity of the helix, suggests a possible directing effect of fluorinated SDA molecules towards an ordered incorporation of the Mg dopants. More realistic models of the dopant-SDA interaction corresponding to a fully loaded Mg-AFI channel are being investigated.

Acidity results

The acidity of the calcined samples has been assessed by pyridine adsorption, and characterised by FTIR spectroscopy. Figure 8 shows infrared spectra in the region of hydroxyl stretching of samples activated in vacuum at 623 K, and after pyridine adsorption and evacuation at 423, 523 and 623 K. Due to the strong absorption of the infrared beam in the high wavelength range, poor quality spectra have been obtained. Nonetheless, two bands can be distinguished in all spectra: a narrow band at ca. 3670 cm^{-1}, that is attributed to terminal P-OH groups, and a broad band centred at about 3500 cm^{-1}, corresponding to bridging Mg-OH-P hydroxyls [15,16,17]. After adsorption of pyridine and evacuation at 423 K, the intensity of both bands is strongly decreased. When the samples are subsequently evacuated at 523 K and 623 K, a progressive increase of the intensity of the band at 3670 cm^{-1} is observed, to reach the original intensity in the spectra recorded after evacuation at 623 K, while only a small change is observed in the intensity of the band at 3500 cm^{-1} with the evacuation temperature. This results evidence the higher acid strength of the bridging hydroxyls as compared to the terminal P-OH groups.

The difference spectra in the region of adsorbed pyridine ring vibration bands have been plotted in figure 9 for sample MgAPO-5-ofbpm, as an example. Similar results were obtained for all the calcined MgAPO's. Five main bands are observed in this region of the spectra, at 1635, 1609, 1544, 1490 and 1447 cm^{-1}, characteristic of pyridine bound to both Brønsted and Lewis acid sites. The bands at 1609 and 1447 cm^{-1} are indicative of pyridine coordinated to Lewis sites. This centres should be assigned to Mg^{2+} sites, as the bands corresponding to pyridine coordinated to Al^{3+} in MgAPO's appear at higher wavenumber values (1620 and 1455 cm^{-1}, respectively) [18]. In contrast to results reported by Müller et al. on MgAPO's [17], we observe bands corresponding to protonated pyridine (1635 and 1544 cm^{-1}), as expected from the decrease in intensity observed for the hydroxyl bands upon pyridine adsorption. In order to calculate the relative concentration of acid sites in the calcined samples, the integrated absorbance of bands at 1544 (Brønsted sites) and 1447 cm^{-1} (Lewis sites) have been calculated. These values, normalized by the sample thickness (integrated area, in cm^{-1}, divided by sample thickness, in $g \cdot cm^{-2}$), are reported in Table 2. Those data indicate that samples MgAPO-5-ofbpm and MgAPO-5-mfbpm possess notably higher concentrations of Brønsted acid sites than samples MgAPO-5-TEA and MgAPO-5-bpm. The total concentration of Brønsted sites, determined after desorption at low temperature (423 K), for sample MgAPO-5-ofbpm is higher than that of sample MgAPO-5-mfbpm. However, there is a higher proportion of strong sites in sample MgAPO-5-mfbpm, as indicated by the higher absorbances determined as the evacuation temperature increases. All the samples possess similar concentration of Lewis sites, except sample MgAPO-5-mfbpm which has a slightly higher concentration. The intensity of the bands associated with the Lewis sites decreases strongly as the evacuation temperature increases, thus indicating that these centres possess a relatively low acid strength. These results are not expected for Al^{3+} centres, and therefore

support the assignment made above for the coordinately bonded pyridine bands, as Mg^{2+} centres would exhibit a weaker Lewis acid strength than Al^{3+}.

Catalytic activity

Results of the catalytic performance of these samples in the reaction of cyclohexene oxide with ethanol are presented in Table 3. It can be observed that samples synthesized with fluorine-containing SDAs (MgAPO-5-ofbpm and MgAPO-5-mfbpm) present a remarkably higher activity than samples synthesized with TEA (MgAPO-5-TEA) or with the non-fluorinated template (MgAPO-5-bpm). The intrinsic activity (turnover number, normalised to the Mg content) is 5-7 times higher in the former samples. The selectivity to trans-2-ethoxi-cyclohexanol (**2**) is almost 100 % in all cases, and only at very high cyclohexene oxide conversions, traces of other products are observed. In none of the experiments e.e. above 5% was observed.

Discussion

The bpm molecule has proven to be an appropriate SDA for directing the crystallization of materials with AFI topology. Indeed, it allows the isomorphous substitution of Mg for Al in the framework, and the resulting materials behave distinctly as compared with MgAPO-5 synthesized using a common agent as TEA. Bpm and TEA-MgAPO-5 as-made materials contain similar amounts of Mg, however they strongly differ in the concentration of acid sites and in the catalytic activity. The acidity and activity of the materials synthesized from fluorine derivatives of bpm are much higher than those of the samples prepared from non-fluorinated bpm and TEA. This suggests that the amount of Mg cations that remain in framework position after removal of the SDA is higher for the fluorine derivatives. It is well known that a large fraction of framework Mg is removed by calcination of the corresponding MgAPO materials synthesized from more conventional template molecules [9], and the extent of the Mg leaching process seems to increase with the Mg concentration in the framework. In

our case, the Mg content of the framework is similar in all samples. However, those synthesized from TEA and bpm present a low resistance against the removal of this cation from the framework, as it is evidenced by the total acidity measured by pyridine adsorption. It is interesting to notice that TEA and bpm differ in their ability to rotate inside the AFI channel. TEA molecules can presumably rotate with no restriction inside the pores, as a bulkier cation like methylsparteinium has been reported to be rotationally "free" inside the pore of SSZ-24, the silica analogue of the AFI topology [19]. On the contrary, the computational study shows the bpm dimers cannot rotate freely inside the channel once the SDA helix is formed. Hence, it could be concluded that the rotational freedom of the SDA molecule would not influence directly the Mg distribution in the framework. However, the theoretical calculations show that there is not a clear preferred orientation of the bpm dimers with respect to the Mg present in the framework. On the contrary, the presence of one fluorine atom in either ortho or meta position of the bpm aromatic ring produced a stronger directing effect on the location of Mg cations in the framework: fluorine and Mg locate on opposite sides of the main AFI channel. According to the acidity and catalytic data, this Mg ordering in the framework enhances remarkably the average thermal stability of the tetrahedral metal cations.

The presence of such a relationship between the location of acid sites and the configuration of the template inside the channels opens the question of whether the Mg distribution in the crystals along the channel wall at nanometric scale could eventually be governed by the spatial configuration of the dimers in the pores. The computational studies show that the dimeric units of the template adopt a stable helicoidal arrangement along the c axis, and the helix handedness is the same for every channel filled up with the intrinsically chiral dimeric bpm units. The reaction of the epoxide (**1**) with ethanol gives two different reaction products, each of them with the corresponding enantiomeric pairs. Therefore, it

would be possible to think that the enantiomeric distribution of acid sites within the framework could eventually lead to enantiomorphic-rich reaction products. Figure 10 presents the chromatogram of two aliquots obtained during an experiment carried out with sample MgAPO-5-mfbpm, at 353 K. In the first one, which corresponds to zero reaction time (before the addition of the catalyst) we can observe the peaks corresponding to the two reactants and the internal standard used (tetradecane). The second one corresponds to a mixture of reactants and products after 48 h of reaction. It can be seen that almost all the reagents have disappeared and the peak corresponding to the epoxide opening is the main product together with traces of minor products. The analysis of this mixture in the chiral column, described in the experimental part, is presented in the inset of Figure 10, where it can be observed that the two enantiomers of the main product can be resolved adequately. We have not detected so far any enantiomeric enrichment of the two chiral products, i.e., a racemic mixture is obtained. One obvious explanation for this result is that no true chiral configuration of acid sites is actually present in the catalysts. However, it has also to be taken into account that no enantiomerically pure chiral porous solid has been prepared so far, and only theoretical prospects have been made on how the intrinsic framework chirality would be transferred to the reacting molecules adsorbed within the pores. Interestingly, it has been reported recently that zeolite beta selectively interacts with the enantiomers of hydrobenzoin (1,2-diphenyl-1,2-ethanediol) [20]. Moreover, molecular simulations stress on the need of using large molecules to display high enantiomeric excesses in separation processes using polymorph A of zeolite beta and the zeotype UCSB-7K [21]. Work is in progress in order to use larger molecules in the reaction of epoxide ring opening to investigate this additional parameter.

Conclusions

Fluorinated and non-fluorinated S-(-)-1-benzyl-2-pyrrolidinemethanol molecules have been found to direct efficiently the synthesis of MgAPO-5 catalysts. These molecules arrange as rigid helices within the channels of the AFI structure, which could lead to a direction of the dopant incorporation; however, it has been found that an association between the dopant and the SDA is also necessary to direct the incorporation of such dopant cations. This association is enhanced for the fluorinated S-(-)-1-benzyl-2-pyrrolidinemethanol molecules, compared to the non-fluorinated one. Samples obtained with fluorinated S-(-)-1-benzyl-2-pyrrolidinemethanol molecules have a higher amount of acid sites, which improves notably their behaviour as acid catalysts.

Acknowledgments

L. Gómez-Hortigüela acknowledges the Spanish Ministry of Education for a PhD grant. The financial support of CICYT (project MAT 2003-07769-C02-02) is acknowledged. We thank Centro de Tecnología Informática for running the calculations. J. Agúndez is acknowledged for his help in the measurements of catalytic activity and T. Blasco for collecting the NMR spectra.

Table 1. Magnesium content calculated by elemental analysis, ^{31}P NMR and EDX, and organic content calculated by TGA. [a] Not measured

Sample (molecule)	Mg/u.c. EA	Mg/u.c. ^{31}P NMR	Mg/u.c. EDX	Organic content (wt %) TGA	Molecules per u.c. TGA
MgAPO-5-bpm	1.16	1.16	0.90	12.43	1.1
MgAPO-5-ofbpm	1.21	1.09	1.08	13.14	1.1
MgAPO-5-mfbpm	1.20	1.14	1.14	12.53	1.0
MgAPO-5- TEA	1.40	1.42	n.m.[a]	9.56	1.6

Table 2. Surface acidity determined by FTIR analysis of adsorbed pyridine. [a] Normalized integrated absorbance of the IR bands of pyridine adsorbed on Brönsted (1545 cm^{-1}) and Lewis (1455 cm^{-1}) acid sites after treatment under vacuum at various temperatures.

Sample	Brönsted sites [a] ($cm \cdot g^{-1}$)			Lewis sites [a] ($cm \cdot g^{-1}$)		
	423 K	523 K	623 K	423 K	523 K	623 K
MgAPO-5-TEA	338	305	262	212	103	53
MgAPO-5-bpm	339	290	231	210	83	35
MgAPO-5-ofbpm	489	355	269	190	58	24
MgAPO-5-mfbpm	445	397	285	245	94	37

Table 3. Results of the catalytic tests.

Catalyst	Time (h)	Conversion of cyclohexene oxide (%)	TON ($mol_{oxide}/eq_{Mg} \cdot h$)
MgAPO-5-TEA	27	7.7	0.093
MgAPO-5-bpm	18	2.8	0.060
MgAPO-5-ofbpm	24	41.1	0.661
MgAPO-5-mfbpm	24	30.6	0.488

Scheme 1. Reaction test.

(**1**) (**2**)

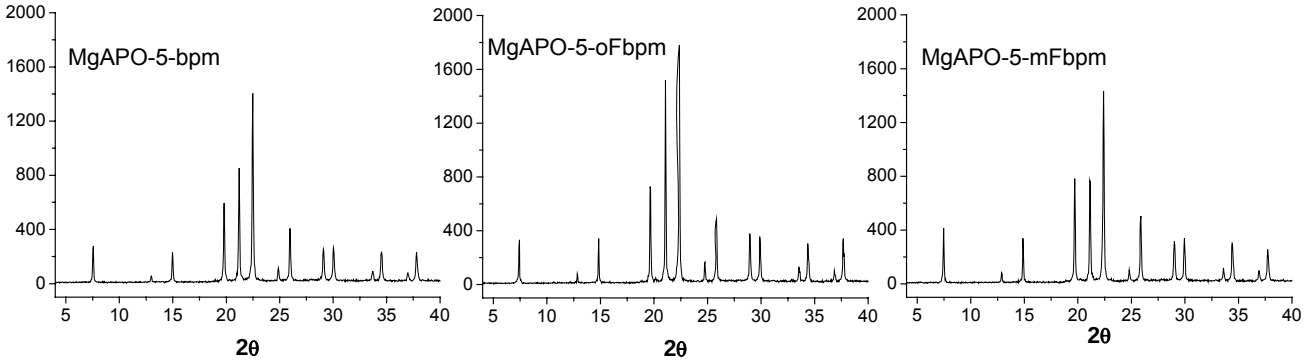

Figure 1. XRD patterns of MgAPO-5 samples sinthesized with S-(-)-1-benzyl-2-pyrrolidinemethanol and its fluorinated derivatives in ortho (ofbpm) and meta (mfbpm) positions.

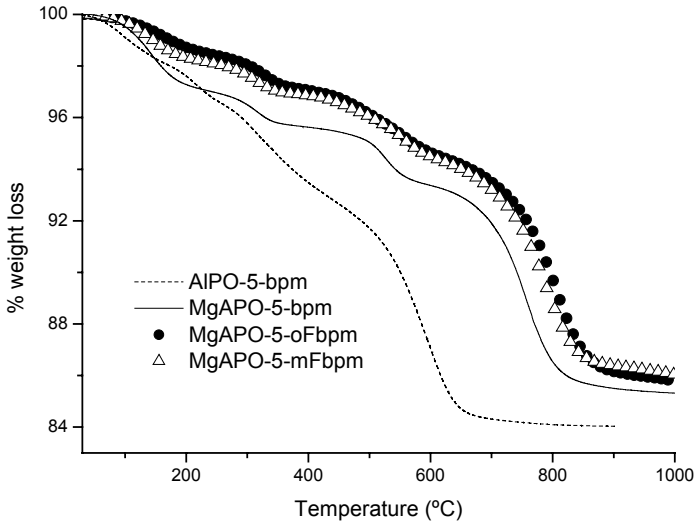

Figure 2. TGA of AlPO-5 and MgAPO-5 samples synthesized with bpm and its fluorinated derivatives as SDA.

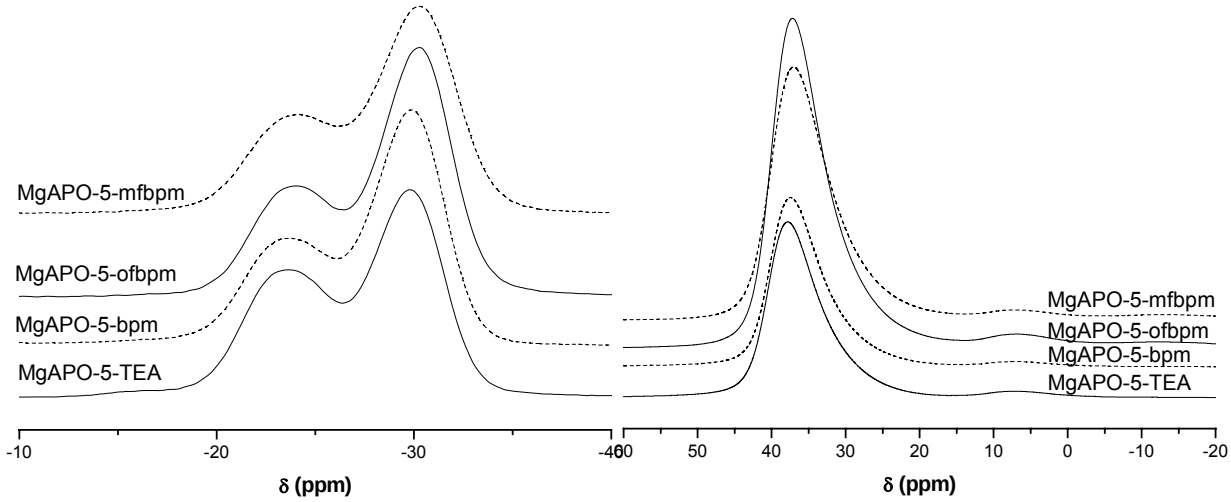

Figure 3. ^{31}P MAS-NMR (left) and ^{27}Al MAS-NMR (right) spectra of MgAPO-5 samples synthesized with TEA, bpm and its fluorinated derivatives as SDA.

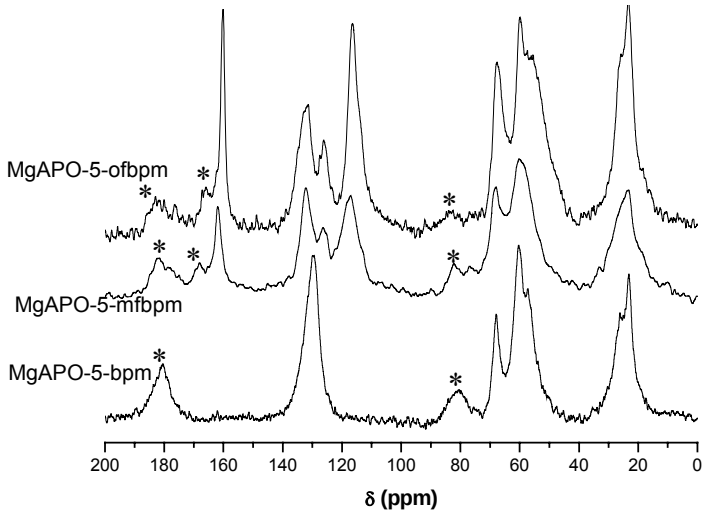

Figure 4. ^{13}C CP-MAS NMR spectra of MgAPO-5 samples synthesized with bpm and its fluorinated derivatives. * indicates rotation bands.

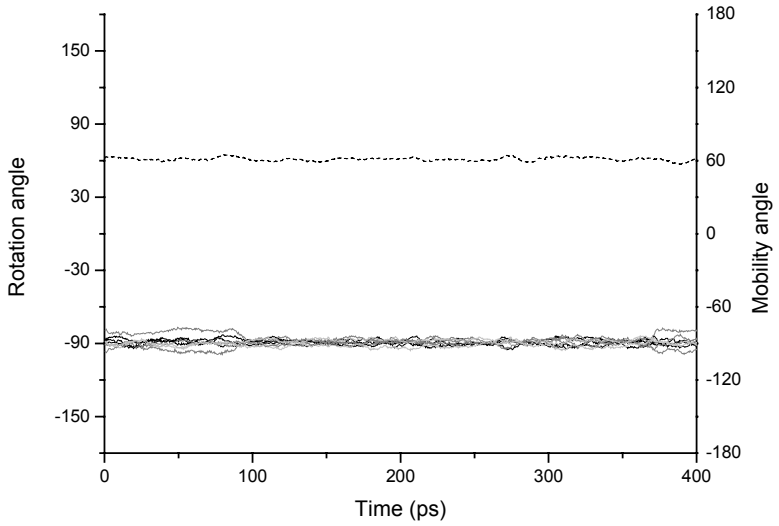

Figure 5. Mobility of the helicoidal arrangement of S-(-)-1-benzyl-2-pyrrolidinemethanol molecules. Grey and black solid lines: angle between consecutive dimers. Dashed line: angle between one of the benzyl planes and one of the 6MR of the channel.

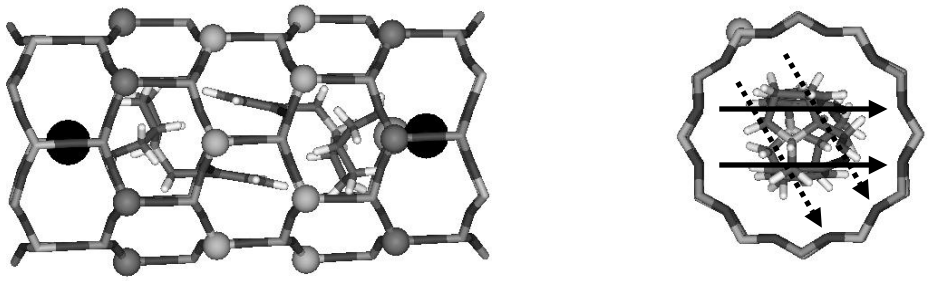

Figure 6. Left: two possible magnesium positions with respect to the dimer: Mg-2 (dark grey atoms displayed as balls) or Mg-1 (light grey atoms displayed as balls); black atoms are argon atoms inserted to preserve intermolecular distance. Right: orientation of ofbpm dimers with respect to magnesium atoms; arrows indicate where the fluorine atoms are pointing towards; solid line arrows: most stable orientation (molecule is drawn in this orientation); dashed line arrows indicate the second most stable orientation.

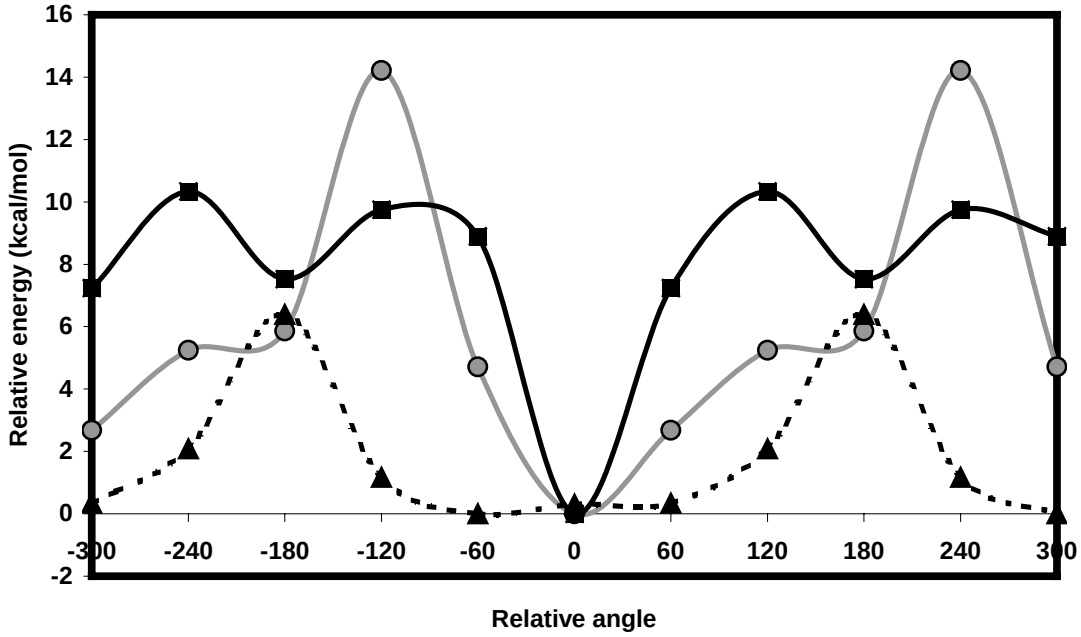

Figure 7. Energy diagram for the rotation of dimers around the c axis with respect to the Mg-1 position. Dashed-black line (triangles): bpm; circles: ofbpm; squares: mfbpm.

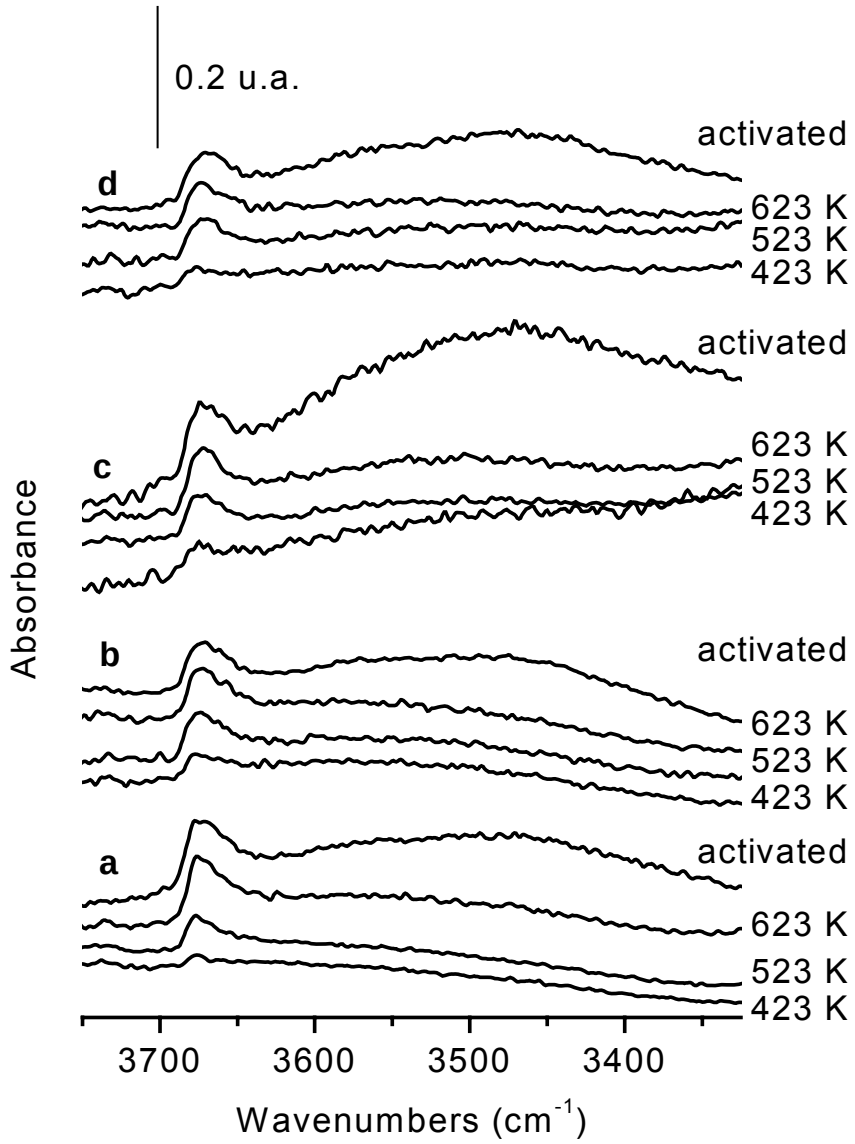

Figure 8. IR-acidity. FTIR spectra of samples (a) MgAPO-5-TEA, (b) MgAPO-5-bpm, (c) MgAPO-5-ofbpm and (d) MgAPO-5-mfbpm activated in a vacuum at 623 K for 9 h, and after pyridine adsorption followed by evacuation at 423, 523 and 623 K.

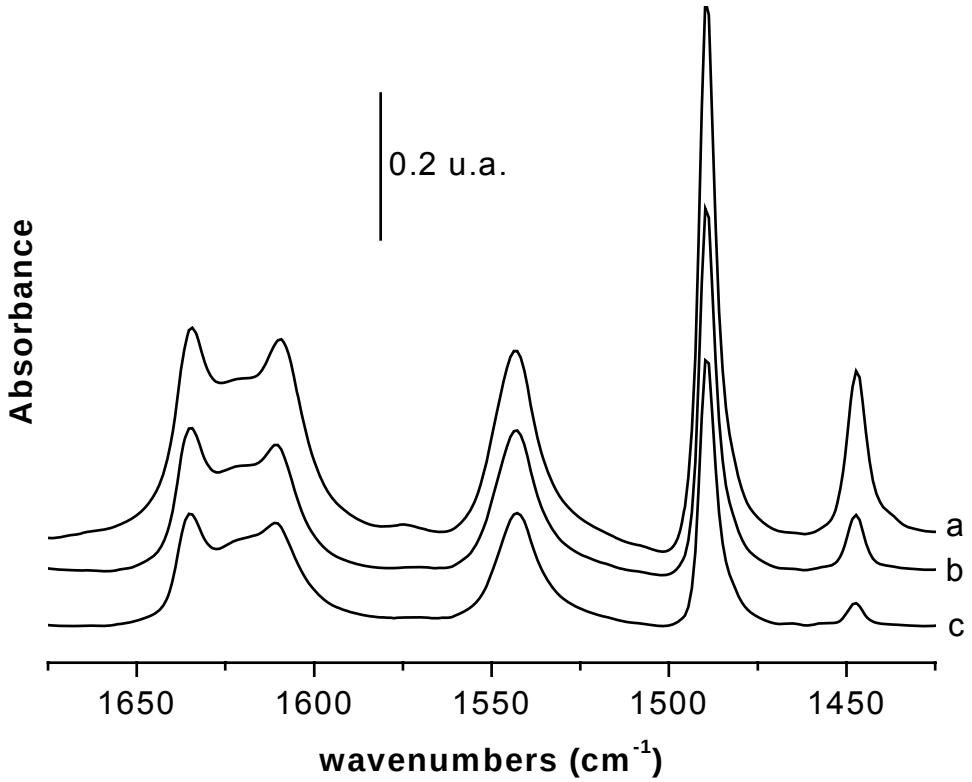

Figure 9. Difference FTIR spectra of sample MgAPO-5-ofbpm after pyridine adsorption followed by desorption at 423 (a), 523 (b) and 623 K (c) in vacuum. The spectrum of the activated sample has been subtracted to every spectrum.

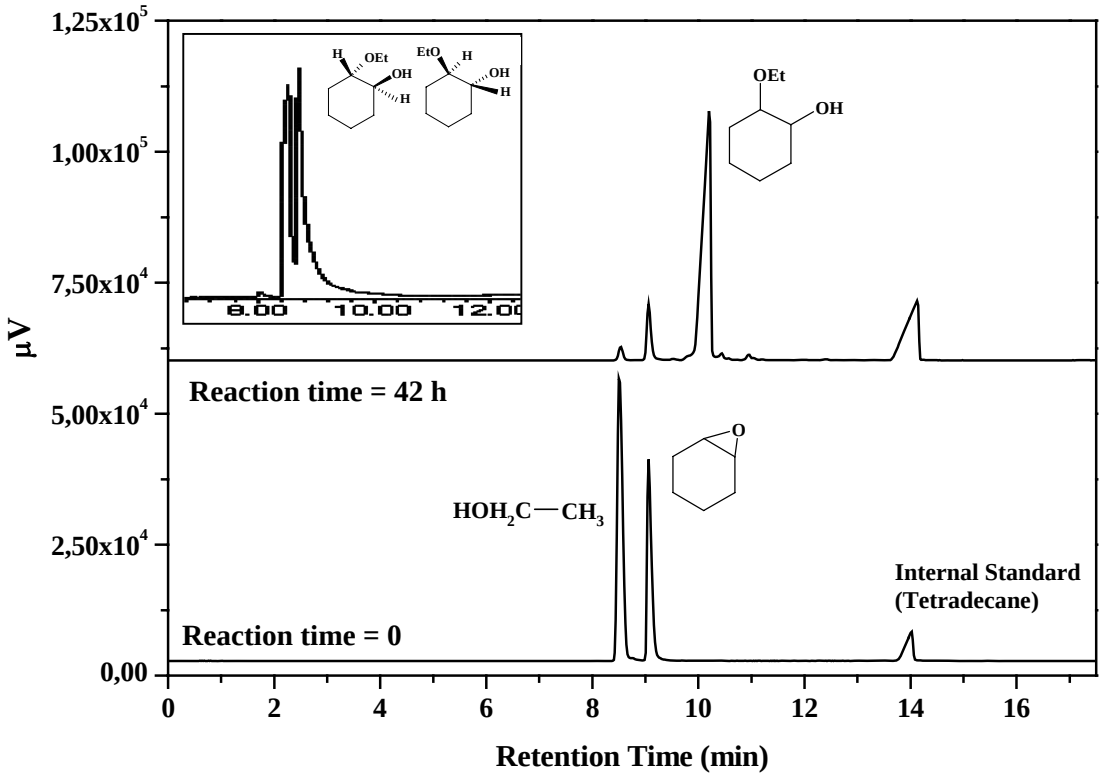

Figure 10. Chromatograms of two aliquots obtained during an experiment carried out with sample MgAPO-5-mfbpm. Bottom: reaction time = 0. Top: reaction time = 42 h. Top-inset: analysis of this mixture in the chiral column.

References

1. A. Corma, Chem. Rev., 95 (1995) 559.

2. R. A. van Santen, G. J. Kramer, Chem. Rev., 95 (1995) 637.

3. D. E. De Vos, S. Ernst, C. Perego, C. T. O´Connor, M. Stöcker, Micro. Meso. Mater., 56 (2002) 185.

4. L. Gómez-Hortigüela, J. Pérez-Pariente, T. Blasco, 14th International Zeolite Conference, book of Abstracts, Cape Town, South Africa, (2004) 407.

5. L. Gómez-Hortigüela, F. Corà, C. R. A. Catlow, J. Pérez-Pariente, J. Am. Chem. Soc., 126 (2004) 12097.

6. L. Gómez-Hortigüela, J. Pérez-Pariente, C. R. A. Catlow, F. Corà. Manuscript in preparation.

7. D. F. Shantz, R. F. Lobo, C. Fild, H. Koller, Stud. Surf. Sci. Catal., 130 (2000) 845.

8. E. Miranda, F. Sánchez, J. Sanz, M. I. Jiménez, I. Martínez-Castro, J. High-Resol. Chromatogr., 21 (1998) 225.

9. P. Concepción, J. M. López-Nieto, A. Mifsud, J. Pérez-Pariente, Zeolites, 16 (1996) 56.

10. L. Gómez-Hortigüela, J. Pérez-Pariente, T. Blasco, Micro. Meso. Mater., 78 (2005) 189.

11. A. Simon, L. Delmotte, J-M. Chezeau, L. Huve, Chem. Comm., 3 (1997) 263.

12. N. J. Peralta-Cruz, S. E. Meza-Toledo, Magn. Reson. Chem., 42 (2004) 81.

13. O. J. B. Nicholas, J. F. Haw, L. W. Beck, T. R. Krawietz D. B. Ferguson, J. Am. Chem. Soc., 117 (1995) 12350.

14. P. Dauger-Osguthorpe, V. A. Roberts, D. J. Osguthorpe, J. Wolff, M. Genest, A. T. Hagler, Proteins: Struct., Function Genetics, 4 (1988) 21.

15. L. Kubelková, S. Beran, J.A. Lercher, Zeolites, 9 (1989) 539.

16. G. Lischke, B. Parlitz, U. Lohse, E. Shereier, R. Fricke, Appl. Catal. A, 166 (1998) 351.

17. G. Müller, J. Bódis, G. Eder-Mirth, J. Kornatowski, J.A. Lercher, J. Mol. Struct., 410-411 (1997) 173.

18. M. da S. Machado, J. Pérez-Pariente, E. Sastre, D. Cardoso, M. V. Giotto, J. L. García-Fierro, V. Fornés, J. Catal., 205 (2002) 299.

19. M. E. Davis, Top. Catal., 25 (2003) 3.

20. M. P. Manning, J. Warzywoda, O. Karahan, A. Sacco, Jr., Stud. Surf. Sci. Catal., 154 (2004) 1957.

21. L. A. Clark, S. Chempath, R. Q. Snurr, Langmuir, 21 (2005) 2267.